arXiv:1511.07890v2 [cond-mat.quant-gas] 8 Jul 2016

η-pairing Superfluid in Periodically-Driven Fermionic Hubbard Model with Strong Attraction

Sota Kitamura and Hideo Aoki
Department of Physics, University of Tokyo, Hongo, Tokyo 113-0033, Japan
(Dated: July 11, 2016)

We propose a novel possibility of dynamically changing the pairing of superconductors from s-wave to η-pairing (where the pairs condense at nonzero momenta) by driving the system with ac fields. We consider a periodically-driven attractive Hubbard model in the strong-coupling regime, and show that the pair-hopping and pair-repulsion terms in the effective Hamiltonian in the Floquet formalism are drastically and separately renormalized, which can change the ground states from an s-wave superconductivity to an η-pairing superconductivity or a charge-ordered phase. While a simple quench scheme would not realize the dynamical phase transition into η-pairing in isolated systems such as cold atoms, we show that there are pathways that realize the dynamical transition, where the field amplitude is varied via a charge-ordered phase as an intermediate state.

PACS numbers: 74.20.Rp, 74.40.Gh, 67.85.-d 71.10.Fd,

I. INTRODUCTION

There are increasing fascinations with periodically-driven systems in condensed-matter and cold-atom physics as an important branch in nonequilibrium physics. Time-periodic external fields have turned out to make dramatic changes in physical properties as efficiently described by the Floquet formalism [1], which provide remarkable developments both in theoretical and experimental studies. A seminal example is the Floquet topological insulator in honeycomb systems [2–4], where a circularly-polarized laser changes the system into a topological one. Further exotic phenomena are proposed with the Floquet formalism [5–8], among which are a dynamical localization and accompanying photo-induced Mott transition [9–12], an attraction-repulsion conversion [13], Floquet topological superconductivity [14], and a modulation of the exchange interaction [15, 16]. Periodic fields can be implemented by a laser light illuminated on electronic systems, or by shaking an optical lattice for cold-atom systems [4].

Now, an intriguing question is: what would be the fate of a superconductor if we apply a periodic driving? One key interest is whether there exists a novel possibility of inducing an exotic superconductivity by driving a conventional superconductor. We provide an answer in the present work by revealing that an exotic, long sought-after "η pairing" [17–21] can indeed emerge in an attractive Hubbard model. The η pairing was originally proposed by C. N. Yang as an eigenstate possessing an off-diagonal long-range order in the Hubbard Hamiltonian [17]. Behind this is an observation that the Hubbard model has, in addition to the usual spin-SU(2) symmetry, another symmetry called η-SU(2) with respect to a pseudospin $\hat{\boldsymbol{\eta}}$ [Eq. (5)]. The η pairing is an exotic condensate with a nonzero expectation value of $\hat{\eta}^x + i\hat{\eta}^y$, which is a fingerprint of a Cooper pair with a nonzero momentum $\boldsymbol{Q} = (\pi, \pi, \cdots)$.

Here we consider the strong-coupling regime of the attractive Hubbard model, where fermions, in equilibrium, form pairs (doublons) in real space and behave as an s-wave fermionic superfluid, as depicted in the left panel of Fig. 1. The possible candidates in real materials we have in mind [22] include $Ba_{1-x}K_xBiO_3$ [23] and doped fullerenes [24]. More direct implementation of the model is expected to be cold-atom systems on optical lattices, where the interatomic interaction can be increased with the Feshbach resonance. Thus hereafter we refer the superconductivity as the fermionic superfluid, in a general context common to condensed-matter and cold-atom systems.

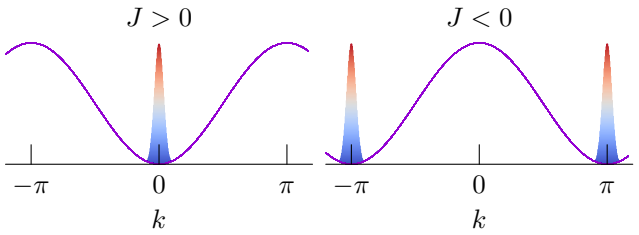

FIG. 1. (color online) Schematic change of the ground state from s-wave pairing for a positive pair-hopping amplitude $J > 0$ to η pairing for a negative $J < 0$ with the band bottom for doublons inverted. Solid line represents the band dispersion, while colored peak symbolizes the occupation of states.

When we perform the strong-coupling expansion of the Hubbard model, we have an effective Hamiltonian for doublons, which comprises pair-hopping and pair-repulsion terms. In ordinary situations the pair-hopping amplitude J is positive, for which the s-wave superconductivity is described as a condensation of doublons in the bottom of bosonic band at $\boldsymbol{k} = \boldsymbol{0}$. If one can invert the sign of the amplitude, this would flip the bandstructure to give a new bottom at $\boldsymbol{k} = \boldsymbol{Q}$, where the exotic, η-pairing superconductivity is expected, as schematically depicted in Fig. 1. While one might imagine such a sign change would be unrealistic, this is in fact feasible in periodically-driven systems: We first show in Sec. II that applying an ac laser field (or shaking the optical lattice) changes the parameters drastically, which enables us to tune them in both magnitude and even in sign.

However, we have to be careful when discussing dynamical phase transitions, because the driven system should in general have a nonequilibrium energy distribution (such as a population inversion), and may not necessarily relax to the ground state. This is important if we have cold atoms in an optical trap, where the system is isolated so that a sudden flipping of the bandstructure will induce an inverted population that is stable in the absence of dissipations.

To overcome this, we propose to invoke a "broken η-SU(2) symmetry", which will turn out to be a peculiar property in the attractive model (as opposed to repulsive half-filled one). While the repulsive Hubbard model is mathematically equivalent to the attractive one at half filling in equilibrium, the equivalence is crucially broken once the driving field is turned on, and results in a breaking of the η-SU(2) symmetry. This brings about richer physics in the attractive case, where the pair-hopping J and pair-repulsion V are modified in different manners due to the phase of the hopping amplitude, which contrasts with the spin-SU(2) invariant repulsive case [15].

Thanks to this, the dynamical instability arises as we shall show in Sec. III: We derive a Gross-Pitaevskii type equation of motion to obtain time evolutions and elementary excitations, which demonstrates that the superfluid phase is unstable against fluctuations in the regime where the pair-repulsion is dominant, while the charge-order becomes unstable when the pair-hopping dominates. These instabilities enables us to manipulate the order parameters, and we actually propose two protocols, a two-step quench and an adiabatic ramping, to realize the η-pairing superfluid, as prescribed in Sec. IV.

II. EFFECTIVE LOW-ENERGY THEORY IN THE STRONG-COUPLING LIMIT

A. Attractive Hubbard model and underlying η-SU(2) symmetry

Let us start from the attractive Hubbard model on a cubic lattice,

$$\hat{H} = -\sum_{ij}^{\text{n.n.}} \sum_{\sigma} t_{ij} \hat{c}^{\dagger}_{i\sigma} \hat{c}_{j\sigma} - U \sum_{i} \hat{n}_{i\uparrow} \hat{n}_{i\downarrow}, \tag{1}$$

in standard notations, where we put the hopping $t_{ij} = 1$ hereafter. For large enough attraction $U > 0$, the ground state tends to maximize the double occupancy and fermions behave as doublons at any filling. The low-energy Hamiltonian for doublons, $\hat{H}_{\text{D}}$, is described by the virtual processes in terms of the strong-coupling expansion (perturbation from $t_{ij} = 0$),

$$\hat{H}_{\text{D}} = -J_0 \sum_{ij}^{\text{n.n.}} \hat{c}^{\dagger}_{i\uparrow} \hat{c}^{\dagger}_{i\downarrow} \hat{c}_{j\downarrow} \hat{c}_{j\uparrow} + V_0 \sum_{ij}^{\text{n.n.}} \frac{\hat{n}_i}{2} \frac{\hat{n}_j}{2}, \tag{2}$$

where $J_0 = 2/U$ is the pair-hopping amplitude, while $V_0 = 2/U$ is the nearest-neighbor pair-repulsion with $\hat{n}_i/2$ being the number of doublons on the i-th site. The ground state is the condensate of doublons, $\prod_i (1 + e^{i\theta} \hat{c}^{\dagger}_{i\uparrow} \hat{c}^{\dagger}_{i\downarrow})|0\rangle$, in the mean-field approximation. We note that at half filling the charge-ordered state, $\prod_{i\in A} (\hat{c}^{\dagger}_{i\uparrow} \hat{c}^{\dagger}_{i\downarrow})|0\rangle$, is also a ground state degenerate with the condensate.

Let us first recall the underlying η-SU(2) symmetry in the Hubbard model: The attractive Hubbard model is known to be equivalent to the repulsive one, since the Shiba transformation [25, 26],

$$\hat{c}^{\dagger}_{j\uparrow} \leftrightarrow (-1)^j \hat{c}_{j\uparrow}, \tag{3}$$

keeps the form of Eq. (1) except for the inverted sign of U. This implies that Eq. (2) is equivalent to a Heisenberg model, which can be seen if we rewrite Eq. (2), up to a constant, as

$$\hat{H}_{\text{D}} = J_0 \sum_{ij}^{\text{n.n.}} (\hat{\eta}^x_i \hat{\eta}^x_j + \hat{\eta}^y_i \hat{\eta}^y_j) + V_0 \sum_{ij}^{\text{n.n.}} \hat{\eta}^z_i \hat{\eta}^z_j, \tag{4}$$

where

$$\hat{\eta}^x_j + i\hat{\eta}^y_j = (-1)^j \hat{c}_{j\uparrow} \hat{c}_{j\downarrow}, \ \hat{\eta}^z_j = \frac{1}{2}(1 - \hat{n}_{j\uparrow} - \hat{n}_{j\downarrow}) \tag{5}$$

is the pseudospin operator that is transformed to the spin operator, $\hat{\boldsymbol{\eta}}_j \leftrightarrow \hat{\boldsymbol{S}}_j$, under the Shiba transformation. Namely, the Hubbard model has, on top of the spin SU(2) symmetry for $\hat{\boldsymbol{S}} = \sum_j \hat{\boldsymbol{S}}_j$, another η-SU(2) symmetry for $\hat{\boldsymbol{\eta}} = \sum_j \hat{\boldsymbol{\eta}}_j$, both in the attractive and repulsive cases.

However, we have to note that the constraint for fixing the particle number breaks the equivalence between attractive and repulsive cases except exactly at half filling, since the chemical potential can be rewritten as a pseudo Zeeman field $\propto \hat{\eta}^z$ along z axis. This makes the usual η-SU(2) symmetry broken, but, more importantly here, ac driving introduces a specific type of η-SU(2) breaking even in half-filled systems as we shall reveal below.

B. Floquet formalism

Let us now turn to a periodic driving of the system. For lattice systems, the Peierls substitution describes the coupling of fermions to ac laser fields as

$$t_{ij} \to t_{ij} e^{i\boldsymbol{A}(t)\cdot\boldsymbol{R}_{ji}} = t_{ij} \sum_{m=-\infty}^{\infty} i^m \mathcal{J}_m(\boldsymbol{A}\cdot\boldsymbol{R}_{ji}) e^{-im\omega t}, \tag{6}$$

where $\boldsymbol{R}_{ji} = \boldsymbol{R}_j - \boldsymbol{R}_i$ with $\boldsymbol{R}_i$ being the position of the i-th site, and $\boldsymbol{A}(t) = \boldsymbol{A}\cos\omega t$ the vector potential of a linearly-polarized laser. On the right-hand side we have performed a Fourier transform, where $\mathcal{J}_m$ is the m-th Bessel function. For cold-atom systems we shake optical lattices, where the vector potential is emulated by $\boldsymbol{A}(t) = \partial_t \boldsymbol{L}(t)$ with $\boldsymbol{L}(t)$ being the periodic motion of the lattice.

If we now apply the transformation (3) to the present case with Eq. (6), resultant repulsive Hamiltonian has a spin-dependent hopping amplitude $t_{ij} e^{-i\sigma\boldsymbol{A}(t)\cdot\boldsymbol{R}_{ji}}$. This degrades the equivalence between the repulsive and attractive cases, and implies that the external field breaks the η-SU(2) symmetry. The breaking of η-SU(2) symmetry becomes significant especially in the strong-coupling limit, since the η-spin becomes the relevant degree of freedom, in terms of which the low-energy Hamiltonian (4) is expressed. However, under a time-dependent drive, the energy is not conserved, so that the usual perturbation scheme to derive Eq. (2) is not applicable.

A key observation here is that we still have a discrete translational symmetry in time since the ac laser field with a driving frequency ω is time-periodic with a period $T = 2\pi/\omega$. Namely, we can employ Floquet's theorem [1]: While we always consider eigenstates of a generator $e^{-i\hat{H}t}$ for temporally

translational-invariant systems, here we can consider eigenstates of the generator for the discrete translation, $e^{-i\hat{F}T} = \mathcal{T}\exp[-i\int_0^T dtH(t)]$, where $\mathcal{T}\exp[\bullet]$ is the time-ordered exponential. The eigenvalue of $\hat{F}$ is called as the quasienergy ϵ, which is the temporal analog of the crystal momentum in Bloch's theorem, and is defined over $(-\omega/2, \omega/2]$. Then the quasienergy eigenstate is expressed as $\Psi(t) = \phi(t)e^{-i\epsilon t}$ with $\phi(t) = \phi(t+T)$.

By expanding $\phi(t)$ and Hamiltonian $\hat{H}(t)$ in Fourier series, the time-dependent Schrödinger equation is converted into a time-independent one,

$$\sum_{l=-\infty}^{\infty} (\hat{H}_{m-l} - m\omega\delta_{m-l})\,\phi_l = \epsilon\phi_m, \tag{7}$$

in the Floquet formalism for an extended Hilbert space, where $\hat{H}_m$ and ϕ_m are the m-th Fourier components of $\hat{H}(t)$ and $\phi(t)$, respectively. Eigenvalues of this matrix are equivalent to those of $\hat{F}$ up to modulo ω.

C. Strong-coupling expansion in the Floquet formalism

To explore the property of the Floquet equation (7) for the periodically-driven Hubbard model, we can perform the strong-coupling expansion in the extended Hilbert space, where the hopping amplitude is decomposed into Fourier components $t_{ij}^{(m)} = i^m \mathcal{J}_m(\boldsymbol{A}\cdot\boldsymbol{R}_{ji})$, which contributes to virtual processes with an energy denominator $U + m\omega$, as depicted in Fig. 2. These contributions via virtual Floquet states modify the original pair-hopping amplitude J_0 and the pair-repulsion V_0 into

$$J_{\rm eff} = \sum_{m=-\infty}^{\infty} (-1)^m \frac{2\mathcal{J}_m(A)^2}{U+m\omega},\ V_{\rm eff} = \sum_{m=-\infty}^{\infty} \frac{2\mathcal{J}_m(A)^2}{U+m\omega}, \tag{8}$$

in time average. Here we take $\boldsymbol{A} = A(1,1,1)$.

We can immediately notice that $J_{\rm eff}$ and $V_{\rm eff}$ are modified in different manners, which is the very manifestation of the broken η-SU(2) symmetry due to the external field. The difference comes from the interference of phase factors: As depicted in Fig. 2, the pair-repulsion term is composed of a virtual fermion hopping from j to i and then back from i to j, which results in a cancellation of phases in a factor $|t_{ij}^{(m)}|^2$. By contrast, the pair-hopping term is composed of a fermion hopping $j \to i$ followed by another $j \to i$, in which the resultant factor, $(t_{ij}^{(m)})^2$, acquires a phase. Thus the two terms have distinct forms due to the phase factors.

This is quite unlike the periodically-driven repulsive Hubbard model at half filling [15], where the effective static Hamiltonian, $\hat{F}_{\rm rep} = V_{\rm eff}\sum_{ij}^{\rm n.n.} \hat{\boldsymbol{S}}_i\cdot\hat{\boldsymbol{S}}_j$, has an isotropically modified exchange interaction $V_{\rm eff}$. In that case all the virtual processes in the strong-coupling expansion have the phase cancellation, leaving the spin-SU(2) symmetry intact.

Let us first examine analytic behavior of the pair-hopping and pair-repulsion terms [Eq. (8)] against the amplitude A and frequency ω of the periodic drive. For $\omega \gg U$, only the $m = 0$ term survives, so that $J_{\rm eff} \sim V_{\rm eff} \sim (2/U)\mathcal{J}_0(A)^2$, which just rescales the energy and nothing interesting happens. Significant difference between $J_{\rm eff}$ and $V_{\rm eff}$ first occurs around $\omega \sim U$ with $\omega - U \gg 1$, where we have asymptotically

$$J_{\rm eff} \sim -\frac{2\mathcal{J}_1(A)^2}{U-\omega},\ V_{\rm eff} \sim +\frac{2\mathcal{J}_1(A)^2}{U-\omega} \tag{9}$$

except in the vicinity of zeros of $\mathcal{J}_1(A)$. If we now look at a numerical result for $J_{\rm eff}$ and $V_{\rm eff}$ against A in Figs. 3 (a) and (b) for two cases of $\omega = 1.2U$ and $\omega = 0.8U$, the parameters indeed change in a manner dramatically sensitive to the value of ω, due to the small denominator. For weak driving we can enhance $J_{\rm eff}$ or $V_{\rm eff}$, while for stronger drives we can even invert the signs of $J_{\rm eff}$ and $V_{\rm eff}$, and vary the ratio $J_{\rm eff}/V_{\rm eff}$ almost arbitrarily.

When we decrease ω even further, drastic changes in the behavior of the parameters occur in a large A region when we are close to $\omega = U/m$, which is due to the diverging contribution from $\mathcal{J}_m(A)^2/(U - m\omega)$. For smaller values of A, we have $J_{\rm eff} \sim (2/U)\mathcal{J}_0(2A)$ and $V_{\rm eff} \sim 2/U$ for $\omega/U \ll 1$ in an ω/U expansion, which is justified only for contributions satisfying $m\omega/U \ll 1$ but other contributions can be neglected due to $\mathcal{J}_m(A) \sim A^m/(2^m m!)$ as far as the small-A region is concerned. This corresponds to the bosonic picture: When ω is small enough, doublons always behave as bosons, where the effective Hamiltonian looks like that of the shaken Bose-Hubbard model [with the hopping renormalized by $\mathcal{J}_0(2A)$]. This is shown in Fig. 3 (c). Thus the characteristic behavior for moderate ω/U regions found above comes from the fermionic nature of the doublon.

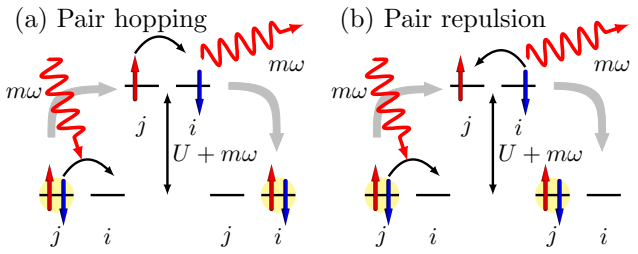

FIG. 2. (color online) Virtual processes for the pair-hopping (a) and the pair-repulsion (b) associated with photoabsorption/emission. Thick gray arrows represent virtual transitions, thin arrows fermion hopping, and wavy lines the coupling to photons.

III. STABILITY ANALYSIS OF THE EFFECTIVE HAMILTONIAN

We have revealed that the parameters in the effective Floquet Hamiltonian can be controlled, in particular we can invert the sign of $J_{\rm eff}$. This urges us to consider an intriguing possibility of the exotic η-pairing superfluid [27], which can be expected from the emergence of a new bandbottom at $\boldsymbol{k} = \boldsymbol{Q} = (\pi,\pi,\pi)$ due to the band flip.

As stressed in Sec. I in discussing dynamical phase transitions, we have to take account of the nonequilibrium distri-

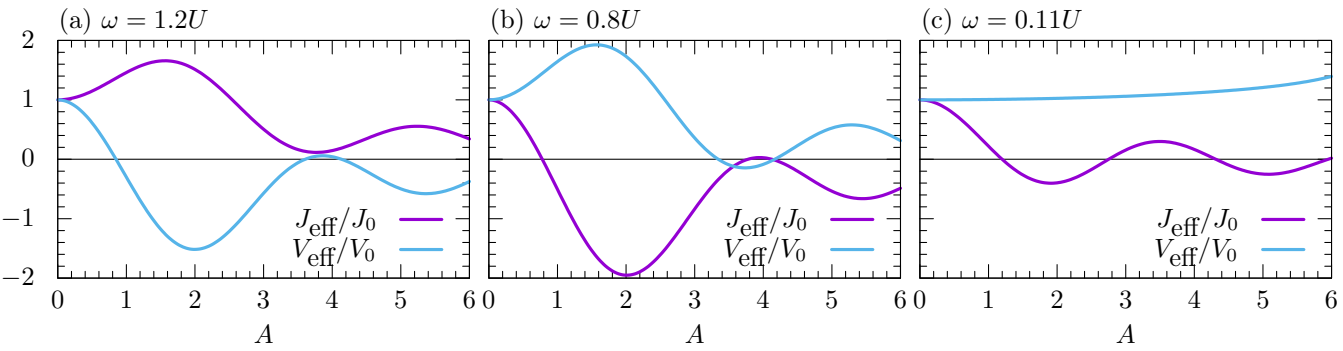

FIG. 3. (color online) Effective pair-hopping $J_{\rm eff}$ and pair-repulsion $V_{\rm eff}$ in the effective Floquet Hamiltonian against the amplitude of the drive A for $\omega = 1.2U$ (a), $\omega = 0.8U$ (b), and $\omega = 0.11U$ (c).

butions, which can make final states totally different from the equilibrium ones especially for isolated systems as in trapped cold atoms. Thus we investigate in this section the stability of the s-wave superfluid under the effective Floquet Hamiltonian. We shall see that the s-wave superfluid does not simply evolve to the η-pairing state, even for the Hamiltonian with negative $J_{\rm eff}$. However, we shall then see that one can induce a collapse of the original superfluid when $V_{\rm eff}$ is dominant, which turns out to be a key for finally realizing the η-pairing state in the discussion in Sec. IV.

A. Elementary excitations

In order to keep track of the fate of s-wave superfluid, here we consider its coarse-grained time evolution by the effective time-evolution operator $e^{-i\hat{F}t}$ with the effective Floquet Hamiltonian,

$$\hat{F} = -J_{\rm eff}\sum_{ij}^{\rm n.n.}\hat{c}^\dagger_{i\uparrow}\hat{c}^\dagger_{i\downarrow}\hat{c}_{j\downarrow}\hat{c}_{j\uparrow} + V_{\rm eff}\sum_{ij}^{\rm n.n.}\frac{\hat{n}_i}{2}\frac{\hat{n}_j}{2}. \tag{10}$$

While the continuous-time evolution with this differs from actual evolution, they are identical at $t = nT$, since $e^{-i\hat{F}T}$ represents the actual time translation by definition.

Then we can discuss the time evolution in the mean-field approximation. Here we describe the superfluid state by a time-dependent ansatz, $|\Psi\rangle = \exp(\sum_j \Psi_j(t)\hat{c}^\dagger_{j\uparrow}\hat{c}^\dagger_{j\downarrow})|0\rangle$, and take a variation $\delta\int dt\,\mathcal{S}(t) = 0$, where $\mathcal{S}(t) = \langle\Psi|(\hat{F} - i\partial_t)|\Psi\rangle/\langle\Psi|\Psi\rangle$. This leads to an equation of motion analogous to the time-dependent Gross-Pitaevskii equation,

$$i\frac{\partial\Psi_i}{\partial t} = \sum_j^{\rm n.n.}\frac{-J_{\rm eff}\Psi_j + J_{\rm eff}\Psi_j^*\Psi_i^2 + 2V_{\rm eff}|\Psi_j|^2\Psi_i}{1+|\Psi_j|^2}. \tag{11}$$

We can easily confirm that the s-wave superfluid is a stationary solution of Eq. (11) for arbitrary external fields, given as $\Psi_0(t) = \Psi_0(0)\exp[-iz((n-1)J_{\rm eff} + nV_{\rm eff})t]$, where n is electron filling and $z = \sum_j^{\rm n.n.} 1$ is the coordination number. This does not necessarily imply that the s-wave superfluid is always stable, as shown below.

The stability of the s-wave superfluid is examined by adding a small perturbation, $\delta\Psi$, to see how it grows. By denoting

$$\Psi_i(t) = \Psi_0(t)\left[1 + \sum_{\boldsymbol{k}}\delta\Psi_{\boldsymbol{k}}(t)e^{i\boldsymbol{k}\cdot\boldsymbol{R}_i}\right], \tag{12}$$

Eq. (11) is linearized into

$$i\frac{\partial}{\partial t}\begin{pmatrix}1 & 0\\ 0 & -1\end{pmatrix}\begin{pmatrix}\delta\Psi_{\boldsymbol{k}}\\ \delta\Psi^\star_{-\boldsymbol{k}}\end{pmatrix} = J_{\rm eff}\begin{pmatrix}\mu_{\boldsymbol{k}}+\sigma_{\boldsymbol{k}} & \sigma_{\boldsymbol{k}}\\ \sigma_{\boldsymbol{k}} & \mu_{\boldsymbol{k}}+\sigma_{\boldsymbol{k}}\end{pmatrix}\begin{pmatrix}\delta\Psi_{\boldsymbol{k}}\\ \delta\Psi^\star_{-\boldsymbol{k}}\end{pmatrix}, \tag{13}$$

where $\mu_{\boldsymbol{k}} = 2\sum_j^{\rm n.n.}\sin^2(\boldsymbol{k}\cdot\boldsymbol{R}_{ji}/2)$, $\sigma_{\boldsymbol{k}} = n(1-n/2)(1 + V_{\rm eff}/J_{\rm eff})\sum_j^{\rm n.n.}\cos(\boldsymbol{k}\cdot\boldsymbol{R}_{ji})$. The diagonalization of Eq. (13) yields a dispersion relation for elementary excitations, which leads to $\omega(\boldsymbol{k}) = J_{\rm eff}\sqrt{\mu_{\boldsymbol{k}}(\mu_{\boldsymbol{k}}+2\sigma_{\boldsymbol{k}})}$ when $\mu_{\boldsymbol{k}} + 2\sigma_{\boldsymbol{k}} > 0$ [28].

If $J_{\rm eff}$ is turned to negative where the η-pairing ground state is expected, the excitation energy $\omega(\boldsymbol{k})$ becomes negative. This would induce a Landau instability when the system is coupled to a heat bath, but in isolated systems nothing will happen to the s-wave superfluid evolving with the effective Hamiltonian.

On the other hand, $\mu_{\boldsymbol{k}} + 2\sigma_{\boldsymbol{k}}$ is not necessarily positive: Indeed it becomes negative for, e.g., $\boldsymbol{k} = \boldsymbol{Q}$ when $V_{\rm eff}/J_{\rm eff} > 1$ at half filling. When $\mu_{\boldsymbol{k}} + 2\sigma_{\boldsymbol{k}} < 0$, the solution becomes $\omega(\boldsymbol{k}) = \pm iJ_{\rm eff}\sqrt{|\mu_{\boldsymbol{k}}|\mu_{\boldsymbol{k}} + 2\sigma_{\boldsymbol{k}}|}$. The imaginary eigenvalue signals a dynamical instability, i.e., a small deviation from an s-wave superfluid grows exponentially.

B. Hamiltonian mechanics formulation

To grasp the physical origin and the fate of the dynamical instability, we can consider a special case where the initial state is uniform on each of sublattice, A and B for a bipartite lattice: Then Eq. (11) becomes coupled equations for $\Psi_A(t)$ and $\Psi_B(t)$. We can then express central quantities of physical interest as the difference in the doublon density (ρ_Q) and in the phase (2θ) between the two sublattices,

$$\rho_Q = \frac{|\Psi_A(t)|^2}{1+|\Psi_A(t)|^2} - \frac{|\Psi_B(t)|^2}{1+|\Psi_B(t)|^2}, \tag{14}$$

$$2\theta = \arg\Psi_A(t) - \arg\Psi_B(t). \tag{15}$$

The superconducting amplitude on each site, $|\langle \hat{c}_{j\downarrow}\hat{c}_{j\uparrow}\rangle|$, is represented as $\{1-[\rho_Q+(-1)^j(n-1)]^2\}^{1/2}/2$. With these variables, Eq. (11) is simplified into

$$\frac{d\rho_Q}{dt} = \frac{\partial H}{\partial \theta}, \quad \frac{d\theta}{dt} = -\frac{\partial H}{\partial \rho_Q}, \tag{16}$$

where

$$H = \frac{z}{2}(n^2-\rho_Q^2)\left[V_{\rm eff} - \sqrt{\frac{(2-n)^2-\rho_Q^2}{n^2-\rho_Q^2}}J_{\rm eff}\cos 2\theta\right]. \tag{17}$$

Namely, the system obeys a Hamiltonian mechanics with respect to ρ_Q and θ as canonical variables with a "classical" Hamiltonian H.

Since Eq. (16) has a form of canonical equation of motion, H is conserved under the time evolution, i.e., the system should evolve along a contour of H, which results in a periodic motion. Figure 4 shows the contour map against ρ_Q and θ for various values of A with a fixed $\omega = 0.8U$. We also show corresponding $(J_{\rm eff}(A), V_{\rm eff}(A))$ on the phase diagram against $J_{\rm eff}, V_{\rm eff}$ in Fig. 5, along with a trajectory when A is varied. Here we consider a half-filled system ($n = 1$).

On the contour maps, the s-wave superfluid is represented by the origin, $(\rho_Q, \theta) = (0, 0)$ [and $(0, \pi)$]. The η-pairing superfluid corresponds to points $(\rho_Q, \theta) = (0, \pm\pi/2)$, while the charge-ordered phases are delineated by $\rho_Q = \pm 1$ as displayed in Fig. 4 (f).

In the absence of the external field [Fig. 4 (a)], $(\rho_Q, \theta) = (0, 0)$ is the fixed point (bottom of the energy profile), which indicates the stability of s-wave superfluid in equilibrium. A parameter quench toward $J_{\rm eff} < 0$ changes the contour map to those shown in Figs. 4 (c)-(e). There, the s-wave superfluid is retained as a fixed point (now at top of the energy profile), so that the dynamical phase transition is not triggered. However, we can notice that a quench toward a region with $V_{\rm eff}/J_{\rm eff} > 1$ (blue in Fig. 5) turns the energy bottom into a saddle point as shown in Fig. 4 (b). This signifies an emergence of the dynamical instability with the system starting to evolve along the emergent contour that starts from the saddle point.

Namely, the dynamical instability of s-wave superfluid results in a collapse of the superfluid phase into an exponential growth of the charge-density wave (CDW) ρ_Q. Because of the integrability of Eq. (17), the motion is periodic; after a long time, the system comes back to the initial s-wave superfluid state. This feature disappears in nonintegrable cases, e.g., the initial state with an inhomogeneity. In such cases the system is expected to be in an equilibrium state for the effective Hamiltonian. We note that this is an approximate description for an evolution over a finite time duration, since in general the final state of the Floquet system after infinite time evolution should tend to be an infinite-temperature state when the higher-order terms in the expansion are considered [29–31].

Now, we note that various other saddle points exist beside that for the s-wave fluid, as marked with red circles in Fig. 4. These are crucial in manipulating the order parameters, as we shall see in the next section. For instance, Fig. 4 (c) implies the existence of a dynamical instability from η-pairing superfluid $[(\rho_Q, \theta) = (0, \pm\pi/2)]$ toward charge-density wave phase. On the other hand, the saddle points in Figs. 4 (d), (e) signify an instability from charge-density wave $[|\rho_Q| = 1]$ into the desired η-pairing superfluid, since $|\rho_Q|$ with $\theta \simeq \pm\pi/2$ decays along the the emergent contour branching off the saddle point (horizontal bold lines) in Figs. 4 (d), (e).

These instabilities are summarized in Fig. 5, as the phase diagram classified by the dynamical instabilities as well as the ground states. There, various regions are characterized by the types of dynamical instabilities described above. We also display the trajectory that represents $(J_{\rm eff}(A), V_{\rm eff}(A))$ when A is adiabatically varied for $\omega = 0.8U$. We can see that the trajectory starts from the s-wave superfluid via the region for instabilities into CDW, then plunges into another region for instabilities into the η-pairing.

IV. NUMERICAL TIME EVOLUTION

We have seen that, while a parameter region for the η-pairing ground state exists, the s-wave superfluid does not evolve to the η-pairing superfluid via the effective Hamiltonian. However, we find that a dynamical-instability channel toward the η-pairing (from CDW rather than from the s-wave) does exist, as well as a channel from the s-wave superfluid into the charge-ordered phase.

This opens a way, by a judicious choice of the temporal variation of the field amplitude, one may be able to induce the evolution finally into η-pairing phase via other phases. A simplest way is to consider a two-step quench of the field amplitude; the first quench inducing a dynamical instability into CDW state, and the second one another instability from CDW to η-pairing. We describe this scheme in Sec. IV A.

Alternatively, we can consider adiabatic ramping (as opposed to quench) of the field amplitude. This approach gives a deeper insight in terms of the classical Hamiltonian dynamics introduced in the previous section, because one can apply the adiabatic theorem for classical mechanics [32, 33]. We shall describe this scheme in Sec. IV B.

Hereafter we concentrate on the half-filled case, but we have confirmed that deviations from half filling do not significantly affect the qualitative behavior. Let us also comment on the time-dependent formalism with a nonperiodic modulation, which we adopt below. Qualitatively, a temporal variation of the field amplitude $A(t)$ can be described by a temporal variation of the effective parameters $J_{\rm eff}(A(t)), V_{\rm eff}(A(t))$. On the other hand, when the Hamiltonian is nonperiodic in time, the Floquet theorem is no longer applicable and the effective Hamiltonian cannot be interpreted as a generator of a discrete time translation. Still, we can take an approach with an effective Hamiltonian by considering the general time-dependent version of the strong-coupling expansion for an arbitrary vector potential. As we show in Appendix A, the system evolves with time-dependent parameters $J_{ij}(t), V_{ij}(t)$ [Eqs. (A5), (A6)], in place of $J_{\rm eff}(A(t)), V_{\rm eff}(A(t))$. In the following we adopt this formalism for numerical calculations.

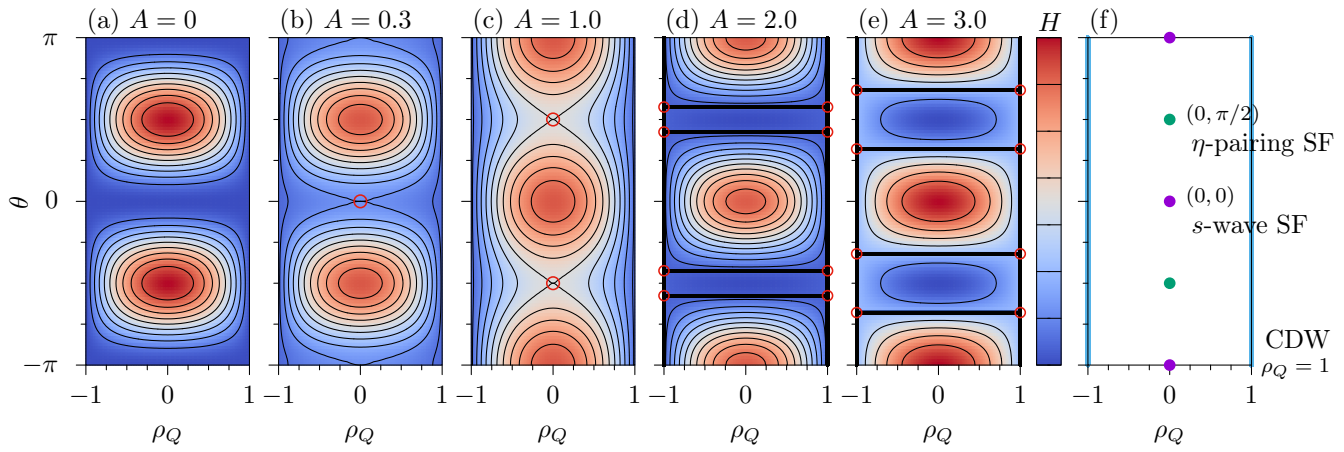

FIG. 4. (color online) Contours of $H \propto (1 - \rho_Q^2)(V_{\rm eff} - J_{\rm eff} \cos 2\theta)$ [Eq. (17)] against ρ_Q and θ for various values of A with a fixed $\omega = 0.8U$ at half filling. Corresponding $(J_{\rm eff}, V_{\rm eff})$ are shown in Fig. 5 below. Saddle points are marked by red circles, and the contours with $H = 0$ are depicted with bold lines in (d), (e). (f) The s-wave superfluid corresponds to $(\rho_Q, \theta) = (0, 0), (0, \pi)$, η-pairing superfluid to $(\rho_Q, \theta) = (0, \pm\pi/2)$, and charge order to $\rho_Q = \pm 1$.

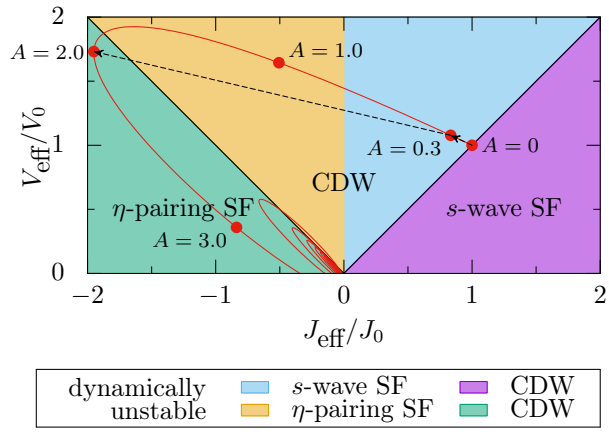

FIG. 5. (color online) The phase diagram of the present system at half filling. Phase boundaries are depicted with black solid lines, while each region is colored based on the types of the dynamical instability as indicated. Red trajectory represents $(J_{\rm eff}(A), V_{\rm eff}(A))$ when A is adiabatically varied for $\omega = 0.8U$. Dotted arrow indicates a path in a quench protocol used in Fig. 6 below.

A. Two-step quench in the field amplitude

Now let us devise the two-step quench protocol to obtain the η-pairing superfluid. We keep track of the evolution of the candidate order parameters,

$$\Delta_0 = \frac{2}{N}\sum_j \langle \hat{c}_{j\downarrow}\hat{c}_{j\uparrow}\rangle \qquad (s\text{-wave pairing}), \quad (18)$$

$$\Delta_Q = \frac{2}{N}\sum_j (-1)^j \langle \hat{c}_{j\downarrow}\hat{c}_{j\uparrow}\rangle \qquad (\eta\text{-pairing}), \quad (19)$$

$$\rho_Q = \frac{1}{N}\sum_{j,\sigma} (-1)^j \langle \hat{c}^\dagger_{j\sigma}\hat{c}_{j\sigma}\rangle \quad \text{(charge-density wave)}. \quad (20)$$

We set $U = 10$, and take an initial state with a tiny inhomogeneity as $\Psi_i(0) = 1 + 0.001\cos(\boldsymbol{q}\cdot\boldsymbol{R}_i)$ with $\boldsymbol{q} = (\pi/6, \pi/6, \pi/6)$.

As the first quench, we turn on the ac field at $t = 0$ with $\boldsymbol{A}(t) = A(t)(1, 1, 1)\sin\omega t$ with $A = 0 \to 0.3$ and $\omega = 8 = 0.8U$ as in Fig. 5 (first part of the dotted arrow). In this situation the dynamical instability occurs from the s-wave superfluid into CDW, as indicated by the blue region ($V_{\rm eff}/J_{\rm eff} > 1$) in Fig. 5 [see also the discussion in the end of Sec. III A]. The numerical result for the time evolution is displayed for $t < 250$ in Fig. 6. A rapid growth of ρ_Q from a small charge inhomogeneity included in the initial state is clearly seen for $t \simeq 50$, which relaxes to a steady charge order for $t \gtrsim 125$ after a complicated transient dynamics.

For comparison we also show the time evolution with the effective static Hamiltonian Eq. (10) for $A = 0.3$. We can see that the collapse of the initial order and subsequent convergence to a final state are roughly described, although some deviations exist in the transient dynamics.

Then we perform the second quench (second part of the dotted arrow in Fig. 5), now from $A = 0.3$ to 2.0 into the region (green in Fig. 5), where the charge order is expected to collapse toward η-pairing superfluid. The numerical result in Fig. 6 for the time evolution after the quench at $t = 250$ clearly shows that this is indeed the case, with a sizable final amplitude close to unity for the η-pairing superfluid.

We can see that relevant order parameters behave as (i) initially $|\Delta_0| \simeq 1$, then (ii) $|\rho_Q| \to 0.8$ in the first quench, and (iii) $|\Delta_Q| \to 0.7$ in the second quench. Thus $|\rho_Q|$ and $|\Delta_Q|$ do not reach unity. This comes from heating effect, which increases for larger change in $|V_{\rm eff}/J_{\rm eff}|$, so that the ratio should be kept closer to unity in the quench protocol if we want to obtain larger Δ_Q. Another way we propose for avoiding heating is an adiabatic ramping of A as described in the next subsection.

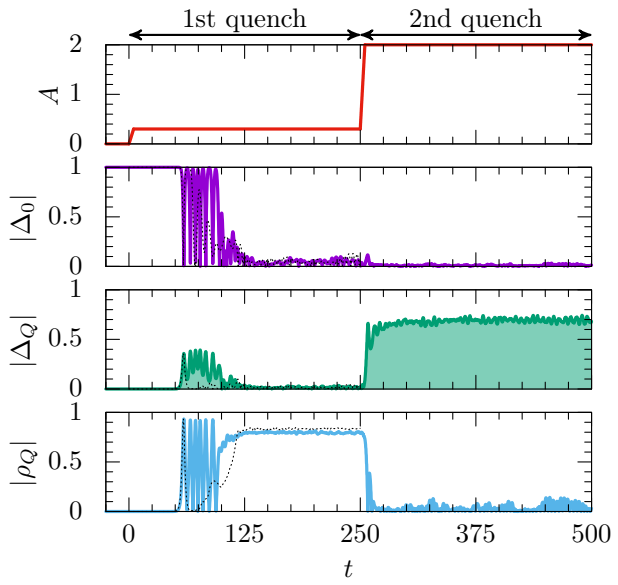

FIG. 6. (color online) Time evolution of the order parameters in a two-step ($t \lesssim 250$) quench protocol (see text) with $U = 10$, $\omega = 8 = 0.8U$. The region where the η-pairing order parameter Δ_Q develops is highlighted in light green. Black dotted lines for $t < 250$ represent the time evolutions by the effective static Hamiltonian Eq. (10).

B. Adiabatic ramping of the field amplitude

Let us alternatively consider an adiabatic change (as opposed to quench) of the amplitude. We again consider a situation where the initial state is uniform on each sublattice, where the dynamics is described by a Hamiltonian Eq. (17). In such a situation we can introduce a classical adiabatic invariant,

$$I = \oint d\theta \rho_Q(\theta), \tag{21}$$

which is conserved in adiabatic changes of parameters according to the adiabatic theorem [32, 33]. The invariant, measured by the area in the phase space enclosed by the trajectory of a periodic motion, is conserved as long as the change of the parameter is much slower than the period of the motion. While the parameters $J_{ij}(t), V_{ij}(t)$ [Eqs. (A5), (A6)] oscillate rapidly, their time averages are approximated by $J_{\rm eff}(A(t)), V_{\rm eff}(A(t))$. Namely, I should be conserved approximately in the coarse-grained dynamics as long as the change of the amplitude is slow enough. Figure 7 illustrates the adiabatic invariant against H for various values of A.

We should remember that the conservation of the adiabatic invariant is broken not only for a rapid change of the amplitude, but even for slow changes when the contour has a saddle point, at which the period of the motion diverges and the change of the amplitude is no longer adiabatic.

Now we consider a protocol in which we perform a ramping up of the amplitude slowly, toward the region where the effective Hamiltonian has η-pairing ground state ($-J_{\rm eff} > V_{\rm eff} > 0$). Here we take $\omega = 0.8U$. As the amplitude is varied, we walk along a trajectory in the phase diagram displayed as the red curve in Fig. 5 aiming at the green region. In the initial stage a dynamical instability arises for the s-wave superfluid, which makes the adiabatic invariant I jump from 0 to about 2π, as can be seen in Figs. 7 (a), (b) (marked with circles). This can also be seen from the area enclosed by the contour containing $(\rho_Q, \theta) = (0, 0)$ [s-wave superfluid] in Figs. 4 (a), (b). After this, I retains this value during the ramping due to the adiabatic theorem. This regime corresponds to a charge order, since the contours [wavy ones along $|\rho_Q| = 1$ in Fig. 4 (c)] for this value of I have large $|\rho_Q|$. [34] The charge order persists as the amplitude is further increased, until we attain $-J_{\rm eff} = V_{\rm eff}$, the phase boundary in Fig. 5.

The situation is then drastically changed due to the charge order collapssing due to the dynamical instability. We can here interpret this in terms of the adiabatic invariant. An emergence of the dynamical instability is signaled as a jump in I: As we increase the amplitude, the maximum value of I against H (at $H = +0$) starts to decrease from 2π as shown in Figs. 7 (d), (e), so that I can no longer be conserved when the maximum becomes below I. When this occurs, the system has $H = +0$ whose contour is, as seen in Fig. 4 (d), a rectangle (marked with bold lines) enclosing $(\rho_Q, \theta) = (0, 0)$. Its corners exactly correspond to the saddle points (four red circles) triggering the dynamical instability.

On the other hand, there is another side-sharing rectangular contour enclosing the η-pairing point, $(\rho_Q, \theta) = (0, \pi/2)$, which belongs to $H = -0$. An increase in the amplitude makes the rectangle for $H = +0$ narrower and that for $H = -0$ wider as the shared side (the horizontal bold line) moves away from $\theta = \pi/2$, as seen in Figs. 4 (d), (e). This leads to a decrease of $I(H = +0)$ accompanied by an increase of $I(H = -0)$.

This observation clearly explains the behavior of the system after passing through the phase boundary. The system is at first in a charge-ordered state with a large I. As we increase the amplitude, the maximum of I decreases until finally hits the conserved value. Then the system starts to evolve along the rectangular contour with $H = +0$. If the amplitude is increased further when the system evolves along the horizontal contour [the bold line in Fig. 4 (d)], the contour drifts away from $\theta = \pi/2$ [see Fig. 4 (e)], and the evolution will be switched to that for $H = -0$ (in the adiabatic limit). Namely, the adiabatic invariant jumps from $I(H = +0)$ to $I(H = -0)$. After this I is conserved with a small value, which results in the large η-pairing amplitude.

Let us now turn to the result of a numerical simulation for the actual time evolution in Fig. 8. We can clearly see that the result indeed excellently agrees with the above argument in that the adiabatic invariant is conserved all the time except at the dynamical instability, i.e., the situations where saddle points appear and the contours with extremely long periods of motion emerge. In the present case the charge-ordered state first appears as a result of a large I, and in the second stage a jump of I toward a small value due to the dynamical instability changes the system into η-pairing superfluid. This way we end up with a large $|\Delta_Q|$ in this protocol as Fig. 8 shows, which actually provides a method alternative to the two-step quench described in Sec. IV A.

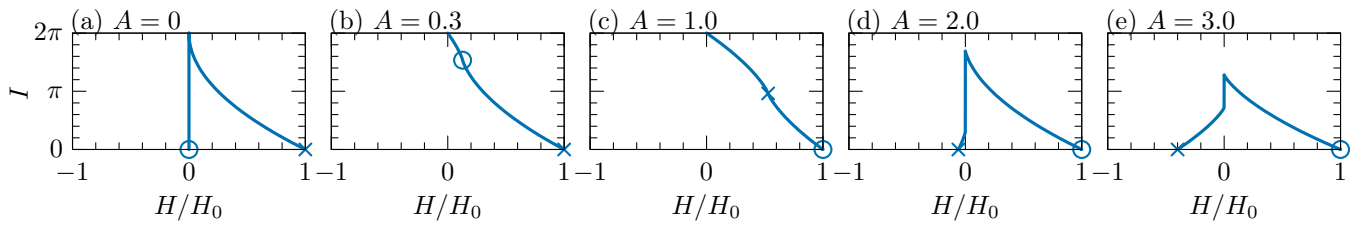

FIG. 7. (color online) The adiabatic invariant I against H [Eq. (17)] for various values of A employed in Fig.4. The invariant for the contours that contain $(\rho_Q, \theta) = (0, 0)$ (s-wave superfluid) are marked with circles, while those containing $(\rho_Q, \theta) = (0, \pi/2)$ (η-pairing superfluid) with crosses. The charge-order ($|\rho_Q| = 1$) corresponds to $H = 0$. H is normalized here by $H_0 = (z/2)(|J_{\rm eff}| + |V_{\rm eff}|)$.

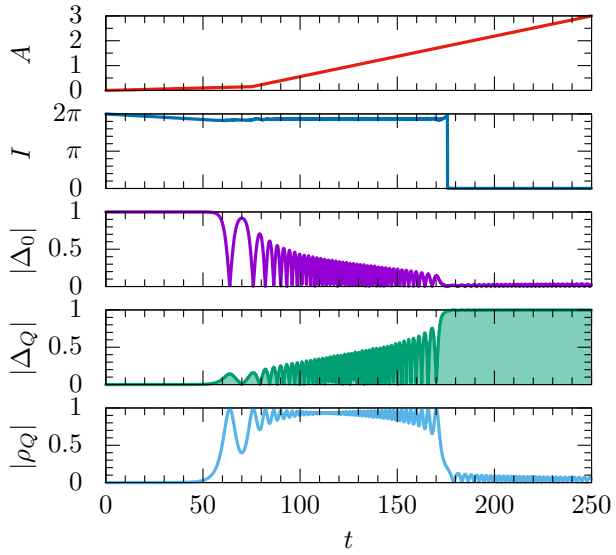

FIG. 8. (color online) Time evolution of the adiabatic invariant (I) and order parameters in an adiabatic protocol for A with $U = 10$ and $\omega = 8 = 0.8U$. The region where Δ_Q develops is highlighted in light green. In this simulation, the ramping rate is increased at $t = 75$ to shorten the simulation time.

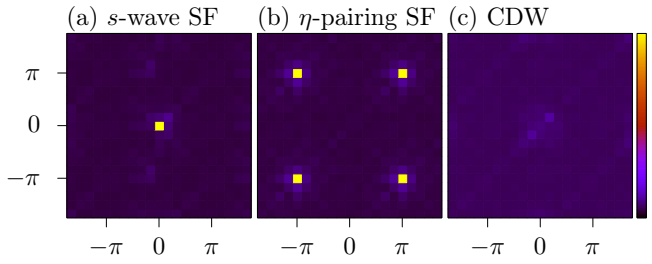

FIG. 9. (color online) Simulated time-of-flight images for an s-wave superfluid (a), an η-pairing superfluid (b), and a charge-density wave state (c).

V. SUMMARY AND EXPERIMENTAL IMPLICATIONS

In this paper we have examined dynamical phase transitions in the periodically-driven large U attractive Hubbard model to look for exotic phases. The effective theory is described by the pair-hopping and pair-repulsion, which are found to be widely tuned, both in magnitude and sign. Thanks to a broken η-SU(2) symmetry induced by the external field, rich possibilities do emerge, in a sharp contrast to the repulsive half-filled case. We have revealed the emergence of the dynamical instabilities between superfluid phases and charge-ordered phase, which induce a dynamical phase transition even in isolated systems. Most importantly, we have invoked dynamical transition as a key process to realize the η-pairing superfluid, for which we have proposed and confirmed numerically two protocols, a two-step quench and an adiabatic ramping of the field intensity.

In this study we have employed several approximations. One is to consider the leading-order tems in the strong-coupling expansion, which can be improved by proceeding to higher orders, or by employing the nonequilibrium dynamical mean-field theory [35]. Another is the mean-field approximation, where we assume that the spatial dimension is sufficiently large. Applications of the present idea with more quantitative methods or to lower-dimensional systems are interesting future problems.

Let us finally comment on the experimental feasibility, where a most promising candidates are cold-atom systems. We can manipulate the strength of attractive interaction with the Feshbach resonance, while the shaken optical lattice has become an established method, as in an experimental realization of the Floquet topological insulator [4].

An evidence for the η pairing proposed in the present paper should be detected in the time-of-flight image of doublons for the cold-atom systems: The image directly reflects the distribution of total momenta of the Cooper pairs, $n_{\rm D}(\boldsymbol{p}) = \langle \hat{\Delta}^\dagger_{\boldsymbol{p}} \hat{\Delta}_{\boldsymbol{p}} \rangle$ with $\hat{\Delta}_{\boldsymbol{p}} = N^{-1} \sum_i \hat{c}_{i\downarrow} \hat{c}_{i\uparrow} e^{-i\boldsymbol{p}\cdot\boldsymbol{R}_i}$. The quantity can be measured in cold-atom experiments, as has been utilized in detecting fermionic superfluids [36].

Figure 9 displays simulated time-of-flight images of doublons. There, we have calculated the total-momentum distribution of doublons (summed over z-axis) for s-wave superfluid, η-pairing superfluid, and CDW. For calculating the expectation value of $n_{\rm D}(\boldsymbol{p})$ we retrieve snapshots of the wave function from the numerical calculation for the amplitude quench [e.g., from $t \sim 375$ in Fig. 6]. We can see in Fig. 9 totally distinct features between different phases: The condensation is signified as sharp peaks at the respective characteristic momenta; $(0, 0)$ for the s-wave superfluid and (π, π) for

the η-pairing superfluid, while for the charge-ordered phase momenta are uniformly distributed.

ACKNOWLEDGMENTS

The authors wish to thank Philipp Werner and Martin Eckstein for illuminating discussions. The present work was supported by a Grant-in-Aid for Scientific Research (Grant No. 26247057) from MEXT and ImPACT project (No. 2015-PM12-05-01) from JST, and by the Advanced leading graduate course for photon science (ALPS) (SK).

Appendix A: Derivation of the time-dependent effective Hamiltonian

Here we derive the time-dependent effective Hamiltonian applicable to nonperiodic amplitude modulations, such as those considered in Sec. IV, with a time-dependent canonical transformation, $e^{-i\hat{S}(t)}$. Let us denote the hopping term in the original Hamiltonian as $\hat{T}(t)$ and the interaction term as $\hat{V}$ to define $\hat{H}_{\rm D}(t)$ as

$$\begin{aligned}\hat{H}_{\rm D}(t) &= e^{i\hat{S}(t)}(\hat{T}(t)+\hat{V}-i\partial_t)e^{-i\hat{S}(t)}\\ &= \hat{V}+\hat{T}(t)+[i\hat{S}(t),\hat{V}]-\partial_t\hat{S}(t)+[i\hat{S}(t),\hat{T}]\\ &\quad+\frac{1}{2}\left[i\hat{S}(t),[i\hat{S}(t),\hat{V}]-\partial_t\hat{S}(t)\right]+\cdots. \end{aligned} \tag{A1}$$

In order to determine $\hat{S}(t)$, we regard it as a series in $\hat{T}$, and impose a condition that $\hat{H}_{\rm D}$ has no first-order terms:

$$\hat{T}(t)+[i\hat{S}(t),\hat{V}]-\partial_t\hat{S}(t)=0. \tag{A2}$$

This differential equation has a formal solution,

$$\hat{S}(t)=e^{-it\mathrm{ad}_{\hat{V}}}\hat{S}(0)+\int_0^t dt' e^{-i(t-t')\mathrm{ad}_{\hat{V}}}\hat{T}(t'), \tag{A3}$$

where $\mathrm{ad}_{\hat{V}}\bullet=[\hat{V},\bullet]$. Then we obtain the effective Hamiltonian up to the second order as $\hat{H}_{\rm D}(t)=(1/2)\hat{P}[i\hat{S}(t),\hat{T}(t)]\hat{P}$, where $\hat{P}$ projects out unpaired fermions. $\hat{S}(0)$ can be determined from a boundary condition $[i\hat{S}(0),\hat{V}]=-\hat{T}(0)$, where the external field is absent for $t\le 0$. This leads to

$$\hat{H}_{\rm D}(t)\sim-\sum_{ij}^{\rm n.n.}J_{ij}(t)\hat{c}^\dagger_{i\uparrow}\hat{c}^\dagger_{i\downarrow}\hat{c}_{j\downarrow}\hat{c}_{j\uparrow}+\sum_{ij}^{\rm n.n.}V_{ij}(t)\frac{\hat{n}_i}{2}\frac{\hat{n}_j}{2} \tag{A4}$$

with

$$\begin{aligned}J_{ij}(t) &= \frac{2}{U}e^{i\boldsymbol{A}(t)\cdot\boldsymbol{R}_{ji}}\cos Ut\\ &\quad+2\int_0^t dt' e^{i(\boldsymbol{A}(t)+\boldsymbol{A}(t'))\cdot\boldsymbol{R}_{ji}}\sin U(t-t'),\end{aligned} \tag{A5}$$

$$\begin{aligned}V_{ij}(t) &= \frac{2}{U}\cos(\boldsymbol{A}(t)\cdot\boldsymbol{R}_{ji})\cos Ut\\ &\quad+2\int_0^t dt'\cos((\boldsymbol{A}(t)-\boldsymbol{A}(t'))\cdot\boldsymbol{R}_{ji})\sin U(t-t').\end{aligned} \tag{A6}$$

For any boundary condition, the first term in Eq. (A3) results in a contribution like $(1/2)\hat{P}i\hat{S}(0)\hat{T}(t)e^{iUt}\hat{P}$, which vanishes in time average [otherwise the expansion is not justified, as seen in, e.g., the divergence of Eqs. (8)], while the second term leads to $J_{\rm eff}, V_{\rm eff}$ [Eqs. (8)] after time average. Namely, if the change of amplitude $A(t)$ is sufficiently slow, the effective Hamiltonian with $J_{\rm eff}(A(t)), V_{\rm eff}(A(t))$ describes a coarse-grained time evolution which averages out the short timescale $\sim U^{-1}, \omega^{-1}$.

Forms of external fields to which the present formalism is applicable should be restricted from the condition for the expansion be justified. For fast components of $\hat{S}(t)$, the Fourier transform of Eq. (A2) gives $i\hat{S}(\nu)\sim-\hat{T}(\nu)/\nu$ with a frequency ν, which should justify the truncation of higher orders in Eq. (A1). For slow components, on the other hand, negligible $\partial_t\hat{S}(t)$ reduces Eq. (A2) to that for static problems, which is justified for strong couplings. The expansion can break down when the second and third terms in Eq. (A2) nearly cancel with each other, unless $\hat{T}(\nu)$ is small enough. This occurs when ν is close to U, although even in such cases $\hat{T}(\nu)$ is vanishingly small in the small-A region for periodic modulations.

[1] G. Floquet, Ann. Sci. École Norm. Supér. **12**, 47 (1883).
[2] T. Oka and H. Aoki, Phys. Rev. B **79**, 081406 (2009).
[3] T. Kitagawa, T. Oka, A. Brataas, L. Fu, and E. Demler, Phys. Rev. B **84**, 235108 (2011).
[4] G. Jotzu, M. Messer, R. Desbuquois, M. Lebrat, T. Uehlinger, D. Greif, and T. Esslinger, Nature **515**, 237 (2014).
[5] A. G. Grushin, A. Gómez-León, and T. Neupert, Phys. Rev. Lett. **112**, 156801 (2014).
[6] R. Wang, B. Wang, R. Shen, L. Sheng, D. Xing, and S. Y. Savrasov, Europhys. Lett. **105**, 17004 (2014).
[7] Z. Zheng, C. Qu, X. Zou, and C. Zhang, Phys. Rev. A **91**, 063626 (2015).
[8] M. Nakagawa and N. Kawakami, Phys. Rev. Lett. **115**, 165303 (2015).
[9] D. H. Dunlap and V. M. Kenkre, Phys. Rev. B **34**, 3625 (1986).
[10] A. Eckardt, C. Weiss, and M. Holthaus, Phys. Rev. Lett. **95**, 260404 (2005).
[11] N. Tsuji, T. Oka, and H. Aoki, Phys. Rev. B **78**, 235124 (2008).
[12] T. Mikami, S. Kitamura, K. Yasuda, N. Tsuji, T. Oka, and H. Aoki, Phys. Rev. B **93**, 144307 (2016).
[13] N. Tsuji, T. Oka, P. Werner, and H. Aoki, Phys. Rev. Lett. **106**, 236401 (2011).
[14] A. Kundu and B. Seradjeh, Phys. Rev. Lett. **111**, 136402 (2013).
[15] J. H. Mentink, K. Balzer, and M. Eckstein, Nat. Commun. **6**, 6708 (2015).
[16] R. Mikhaylovskiy, E. Hendry, A. Secchi, J. H. Mentink, M. Eckstein, A. Wu, R. Pisarev, V. Kruglyak, M. Katsnelson, T. Rasing, and A. Kimel, Nat. Commun. **6**, 8190 (2015).
[17] C. N. Yang, Phys. Rev. Lett. **63**, 2144 (1989).
[18] A. Kantian, A. J. Daley, and P. Zoller, Phys. Rev. Lett. **104**,

240406 (2010).
[19] A. Rosch, D. Rasch, B. Binz, and M. Vojta, Phys. Rev. Lett. **101**, 265301 (2008).
[20] M. Di Liberto, C. E. Creffield, G. I. Japaridze, and C. Morais Smith, Phys. Rev. A **89**, 013624 (2014).
[21] A. Bermudez and D. Porras, New J. Phys. **17**, 103021 (2015).
[22] FeSe [37] would also be interesting in that the material is in the BCS-BEC crossover region with the size of the superconducting gap as large as the Fermi energy.
[23] V. Meregalli and S. Y. Savrasov, Phys. Rev. B **57**, 14453 (1998).
[24] F. C. Zhang, M. Ogata, and T. M. Rice, Phys. Rev. Lett. **67**, 3452 (1991).
[25] H. Shiba, Prog. of Theor. Phys. **48**, 2171 (1972).
[26] V. J. Emery, Phys. Rev. B **14**, 2989 (1976).
[27] For cold-atom systems, the η-pairing ground state in the effective Floquet Hamiltonian is also investigated with different mechanisms [20, 21].
[28] There is another solution, $-\omega(\boldsymbol{k})$, but it has a negative Bogoliubov norm $|\delta\Psi_{\boldsymbol{k}}|^2 - |\delta\Psi^{\star}_{-\boldsymbol{k}}|^2$. It is physically equivalent to the solution $\omega(\boldsymbol{k})$ with a positive Bogoliubov norm.
[29] L. D'Alessio and M. Rigol, Phys. Rev. X **4**, 041048 (2014).
[30] A. Lazarides, A. Das, and R. Moessner, Phys. Rev. E **90**, 012110 (2014).
[31] T. Mori, T. Kuwahara, and K. Saito, Phys. Rev. Lett. **116**, 120401 (2016).
[32] L. D. Landau and E. M. Lifshitz, *Mechanics* (Pergamon, Oxford, 1977).
[33] J. Liu, L. Fu, B.-Y. Ou, S.-G. Chen, D.-I. Choi, B. Wu, and Q. Niu, Phys. Rev. A **66**, 023404 (2002).
[34] When the trajectory is open but periodic in θ, I can still be defined as the area between the trajectory and $\rho_Q = 0$.
[35] H. Aoki, N. Tsuji, M. Eckstein, M. Kollar, T. Oka, and P. Werner, Rev. Mod. Phys. **86**, 779 (2014).
[36] C. A. Regal, M. Greiner, and D. S. Jin, Phys. Rev. Lett. **92**, 040403 (2004).
[37] S. Kasahara, T. Watashige, T. Hanaguri, Y. Kohsaka, T. Yamashita, Y. Shimoyama, Y. Mizukami, R. Endo, H. Ikeda, K. Aoyama, *et al.*, Proc. Natl. Acad. Sci. USA **111**, 16309 (2014).